Structure of the MID1 Tandem B-Boxes Reveals an Interaction Reminiscent of Intermolecular Ring Heterodimers[†,‡]

Hu Tao,[§] Brandi N. Simmons,[§] Suryaparkash Singireddy,[§] Madhu Jakkidi,[§] Kieran M. Short,[||] Timothy C. Cox,[⊥,#] and Michael A. Massiah*[,§]

Department of Biochemistry and Molecular Biology, Oklahoma State University, Stillwater, Oklahoma 74078, Department of Biochemistry and Molecular Biology and Department of Anatomy and Developmental Biology, Monash University, Clayton, Victoria, Australia 3800, and Division of Craniofacial Medicine, Department of Pediatrics, University of Washington, Seattle, Washington 98195

Received September 10, 2007; Revised Manuscript Received December 18, 2007

ABSTRACT: The tripartite motif (TRIM) protein family, defined by N-terminal RING, B-box, and coiled-coil (RBCC) domains, consists of either a single type 2 B-box domain or tandem B-box domains of type 1 and type 2 (B1B2). Here, we report the first structure of the B-box domains in their native tandem orientation. The B-boxes are from Midline-1, a putative ubiquitin E3 ligase that is required for the proteosomal degradation of the catalytic subunit of protein phosphatase 2A (PP2Ac). This function of MID1 is facilitated by the direct binding of Alpha4, a regulatory subunit of PP2Ac, to B-box1, while B-box2 appears to influence this interaction. Both B-box1 and B-box2 bind two zinc atoms in a cross-brace motif and adopt a similar $\beta\beta\alpha$ structure reminiscent of the RING, PHD, ZZ, and U-box domains, although they differ from each other and with RING domains in the spacing of their zinc-binding residues. The two B-box domains pack against each other with the interface formed by residues located on the structured loop consisting of the two antiparallel β-strands. The surface area of the interface is 188 Å^2 (17% of the total surface). Consistent with the globular structure, the T_m of the tandem B-box domain (59 °C) is higher than the individual domains, supporting a stable interaction between the B-box 1 and 2 domains. Notably, the interaction is reminiscent of the interaction of recently determined RING dimers, suggesting the possibility of an evolutionarily conserved role for B-box2 domains in regulating functional RING-type folds.

B-box domains are found in hundreds of proteins but are a distinct feature of the tripartite motif (TRIM)[1] proteins, which are defined by their N-terminal RING, B-box, and coiled-coil (RBCC) domains. Many RBCC/TRIM proteins have a single B-box (B-box type 2) domain; however, some have tandem domains with a type 1 B-box domain (B-box1) located N-terminal to the B-box2 domain (*1*). In the cases of non-TRIM proteins, the B1B2 order of tandem B-box domains is also conserved, suggesting a degree of cooperative function throughout evolution. The two types of B-box domains are cysteine- and histidine-rich, and although they each have distinct zinc-binding consensus sequences and sizes, they have both recently been shown to bind two zinc atoms with similar secondary and tertiary structures (*1*−*3*). B-box2 domains are smaller by ∼8 amino acids with either eight classical zinc-binding residues or seven classical residues and one non-classical aspartic acid to coordinate a zinc (*3*).

Despite the large number of proteins with B-box domains, very little is known about their structure and function within the proteins in which they are located. Distinct functions for B-box domains were first demonstrated with the finding that the B-box1 domain of Midline-1 (MID1) and Midline-2 (MID2) specifically bound Alpha4 (*4*), a regulator of the catalytic subunit of protein phosphatase 2A (PP2Ac) (*4*−*6*). Interaction with MID1/MID2 tethers Alpha4 to the microtubule cytoskeleton and likely facilitates recruitment of PP2Ac to these complexes, where it can target specific substrates and itself is marked by ubiquitin for proteosome-mediated degradation (*4*, *6*, *7*). Although B-box1 is responsible for directly binding Alpha4, the presence of the B-box2 domain of MID1 does impact the affinity between B-box1

[†] This work was supported in part by the Oklahoma State University Agricultural Experimental Station (Project 2527), the Oklahoma Center for the Advancement of Science and Technology (HR-196), NSF CAREER (0546506) grants (M.A.M.), and establishment funds from the Department of Pediatrics, University of Washington (T.C.C.).

[‡] PDB accession code for the NOE restraints file and coordinates for 20 structures of MID1 B1B2 is 2jun.

* Corresponding author. E-mail: massiah@biochem.okstate.edu; tel.: (405) 744-3797; fax: (405) 744-7799.

[§] Oklahoma State University.

[||] Department of Biochemistry and Molecular Biology, Monash University.

[⊥] Department of Anatomy and Developmental Biology, Monash University.

[#] University of Washington.

[1] Abbreviations: BRCA1, breast cancer 1 early onset; BARD1, BRCA1-associated RING domain; GST, gluthathione *S*-transferase; HDM2, double minute 2, human homologue (p53 binding protein); HSQC, heteronuclear single quantum coherence; MID1, Midline-1; NMR, nuclear magnetic resonance; NOE, nuclear Overhauser effect; NOESY, NOE spectroscopy; PHD, plectstrin homology domain; PP2Ac, catalytic subunit of protein phosphatase 2A; RING, really interesting new gene; RBCC, RING-B-box-coiled coil; TRIM, tripartite motif; rmsd, root-mean-squared deviation.

10.1021/bi7018496 CCC: $40.75
Published on Web 01/26/2008

and Alpha4 (*6*). The importance of both B-boxes is further highlighted by the fact that mutations within either the B-box1 or the B-box2 domains (ΔCys137, Cys142Ser, Cys145Tyr, Cys195Phe, Ala130Val, and Ala130Ser) of MID1 have been found in patients with Opitz G/BBB syndrome (OS)—a developmental disorder characterized by numerous abnormalities including clefts of the lip and primary palate, cardiac structural defects, and genital anomalies (*8*−*11*). Such mutations are thought to result in loss of MID1 function.

We recently determined the high-resolution structure of the individual domains of B-box1 and B-box2 from MID1 (*2*, *3*). Both B-box1 and B-box2 domains coordinated two zinc atoms in a cross-brace fashion and adopted $\beta\beta\alpha$ RING-like folds commonly associated with E3 ligases (*3*), even though they share little sequence homology with RING domains. The structure of B-box1 contained a hydrophobic cleft between the helix and the two loops involved in zinc coordination that is similar to the surface of the cCbl RING that makes contact with UbcH7. While the MID1 RING domain is presumed to possess E3 ubiquitin ligase activity, the structure of B-box1 suggests either an independent E3 ligase function or a RING-dependent E3-enhancing ligase (i.e., an E4 function) on a single polypeptide chain. However, E3 or E4 ligase function has not yet been demonstrated for the MID1 B-box1 domain. B-Box2, on the other hand, does not show a distinct cleft that could accommodate an E2 enzyme, supporting the notion that B-box2 domains represent a functionally distinct group of B-box domains. However, it remains possible that the B-box2 domain functions to regulate B-box1 or the RING domain in the cases where TRIM proteins have a single B-box domain.

Here, we report the structure of the human MID1 B-box domains in their native tandem orientation (Ser90 to Glu214). The structure of each B-box domain is consistent with the individually determined domain structures; however, in their native tandem orientation, the two B-boxes pack against each other with the interface formed by residues on the structured loop that features the short β-strands. Interestingly, this packing of the B-boxes is reminiscent of the BARD1-BRCA1 and Bmi-1-Ring1B RING intermolecular heterodimers and the HDM2 RING homodimer (*12*−*14*), supporting such a regulatory or modulatory function for B-box2.

MATERIALS AND METHODS

Native human *MID1* cDNA was used as the template to amplify the region encoding residues Ser90 to Glu214 that encompassed B-box1 and B-box2. The PCR fragment was cloned into the pGEX-4T2 plasmid for expression of the tandem B-boxes (B1B2) with an N-terminal glutathione *S*-transferase (GST) tag (GE Healthcare). The orientation and integrity of the vector was verified by DNA sequencing prior to transformation into BL21(*DE3*) cells. Expression and purification of ^{15}N and ^{15}N−^{13}C-labeled B1B2 were similar to methods used for MID1 B-box1 (*2*).

The NMR samples contained ∼0.5 to 1.0 mM ^{15}N− and ^{15}N−^{13}C-labeled B1B2 in ST-buffer (50 mM Tris-HCl, 100 mM NaCl, 1 mM $ZnCl_2$, and 10 mM β-mercaptoethanol), pH 7.5, 2% sodium azide, and 90% H_2O/10% D_2O, respectively. Double and triple resonance NMR experiments were performed at 21 °C (probe temperature) on a Varian Inova 600 MHz spectrometer equipped with a 5 mm triple resonance (^{1}H, ^{13}C, and ^{15}N) probe with *z*-axis gradient, as described previously (*2*). The NMR data were processed with nmrPipe (*15*) and analyzed with SPARKY3 (*16*) using PowerPC G5 Macintosh computers operating with OSX 10.4.

NOEs were grouped as strong, medium, or weak based on their intensities in the 3-D ^{15}N- and ^{13}C-edited NOESY spectra and assigned distance ranges of 1.8−2.8 Å, 1.8−3.3 Å, and 1.8−5.0 Å, respectively. An additional 1.0, 2.3, and 0.5 Å were added to restraints derived from NOEs involving methyl groups (CH_3), aromatic protons, and ambiguous geminal protons (CH_2), respectively. Hydrogen-bond restraints between the carbonyl and the amide groups were defined with two distance restraints (O−H, 1.8−2.5 Å and O−N, 2.7−3.5 Å). Hydrogen bonds were established from NOE patterns and the proximities of donor and acceptor groups in initial structures calculated primarily with NOE-derived restraints. The majority of hydrogen bonds was associated with the secondary structural elements. Using the chemical shifts of ^{1}H, ^{15}N, and ^{13}C atoms for each amino acid, dihedral angles were estimated for 48 amino acids using TALOS (*17*). Distance restraints between the zinc atom and the cysteine side-chain atoms were rigidly fixed to 2.30−2.35 Å (Zn−Sγ) and 3.5 Å (Zn−Hβ). Distances between the zinc atom and the histidine side-chain nitrogen were fixed at 1.95−2.05 Å (*18*, *19*). The distance between the carboxylate Oδ1 oxygen of Asp190 and the zinc atom was fixed at 2.35 Å. To maintain a tetrahedral geometry around the zinc, distances between the Sγ, the Nϵ, and the Oδ1 atoms were set to 3.85 Å (*2*). The number of zinc atoms coordinated by each B-box domain was previously determined using ESI-FTICR and ICP mass spectrometry, Ellman's reagents, Cβ chemical shifts of cysteines, tautomeric states of histidines, and NOE cross-peak patterns (*2*, *3*).

The structures were computed using CYANA 2.1 (*20*) on a PowerPC Quad G5 Macintosh computer. From a total of 200 randomly calculated structures, 20 structures were selected based on low target functions (tf < 1), and low rmsd values for backbone and heavy atom superposition were selected. A total of 20 000 steps for torsion angle simulated annealing were employed.

RESULTS

Comparison of the 2-D ^{1}H−^{15}N HSQC spectra (Figure 1a) of B1B2 with those of the isolated B-box1 and B-box2 domains revealed chemical shift changes for a number of amino acids, indicating that their chemical environments differed. Specifically, 13 amino acids of B-box1 had their NH proton chemical shifts perturbed by 0.15−0.25 ppm, and they included residues Thr110, Leu118, Ala130, Val131, Lys132, Thr133, Val135, Thr136, Cys137, Val139, Tyr141, Leu161, and Ile162 (Figure 1a,b). B-Box2 had 10 residues showing slightly smaller NH proton chemical shift changes (∼0.10 ppm) (Figure 1a,b). The ^{15}N chemical shift changes for the above noted residues were larger (Figure 1). In addition, the comparison of the HSQC spectra of B1B2 and B-box1 revealed that a portion of the overlapped peaks in the B-box1 spectrum (ref *2* and Figure 1) shifted and had to be re-identified. As a result, the NMR assignments and NOEs used for structure calculations had to be completely and independently assigned using double and triple resonance data, as described previously (*2*, *3*).

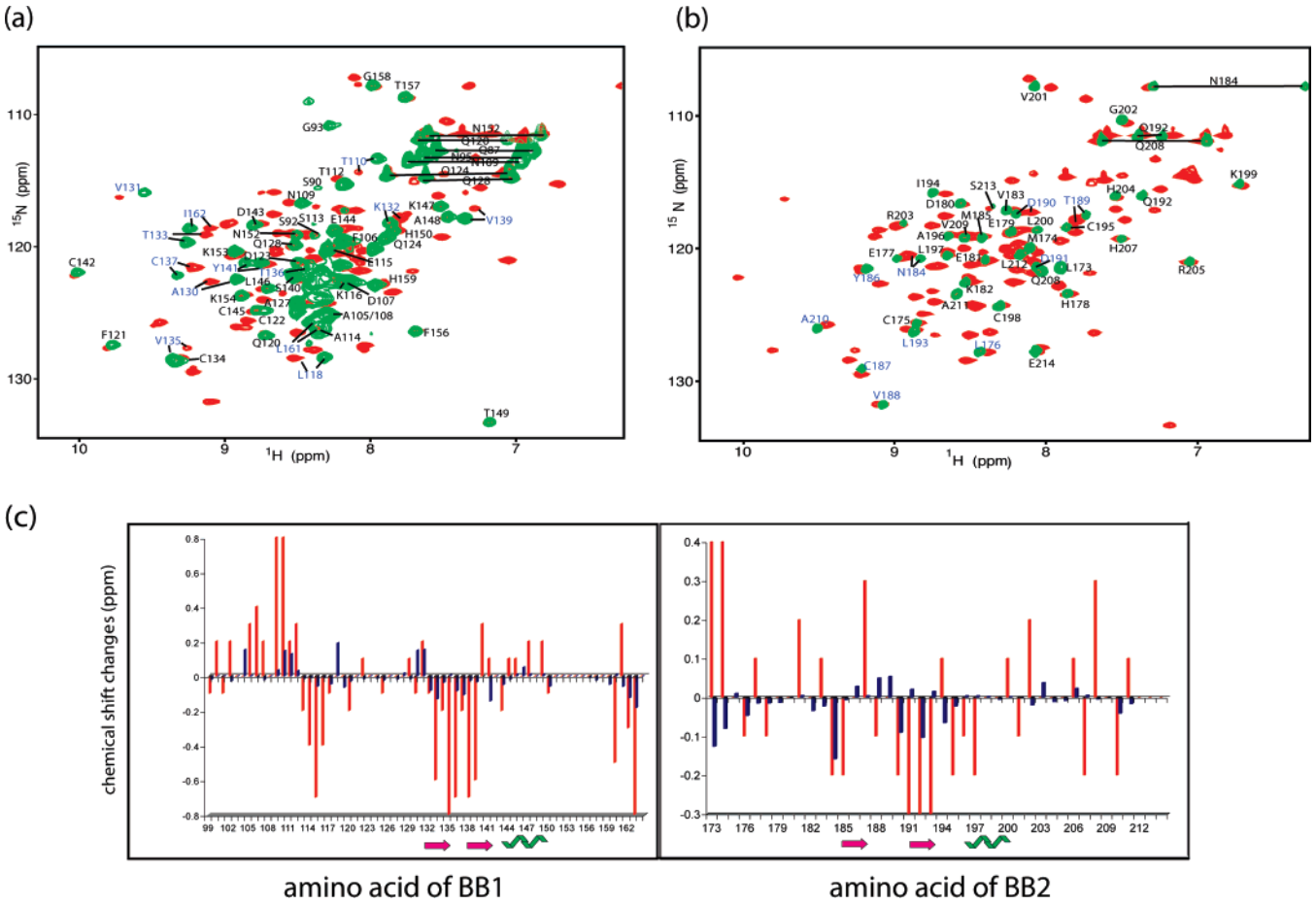

FIGURE 1: Chemical shift changes in the B-box domains (a). Overlay of ^{1}H−^{15}N HSQC spectra of B-box1 (green) and B1B2 (red) performed at 600 MHz and 21 °C. (b) Overlay of ^{1}H−^{15}N HSQC spectra of B-box2 (green) and B1B2 (red). Amino acid assignments of a majority of peaks, corresponding the backbone NH atoms, are shown. Horizontal lines identify side-chain NH_2 groups of glutamine and asparagine residues. The blue labels show the amino acids with altered chemical environments. (c) Changes in NH (blue) and ^{15}N (red) chemical shifts for amino acids in each domain are shown.

Backbone ^{1}H, ^{15}N, and ^{13}C atoms were assigned using the three-dimensional HNCA, HNCACB, CBCA(CO)NH, ^{1}H−^{15}N HSQC-NOESY, and ^{1}H−^{15}N−^{15}N HSQC-NOESY-HSQC spectra. Secondary structural elements of each B-box domain, determined by NOE cross-peak patterns and chemical shift indices, consisted of two short β-strands located on a structured loop and a three-turn α-helix. The first 27 amino acid N-terminal region (Ser90 to Val117), which contained a putative MAP kinase phosporylation site (PNS^{96}P), and the 13 amino acids (Leu161 to Leu173) linking B-box1 and B-box2 were unstructured based on the lack of backbone heavy atom triple resonance connectivities and near-neighbor or long-range NOEs. Each B-box domain in the tandem structure coordinates two zinc atoms in a cross-brace fashion, as seen in the individually determined B-box structures (*2*, *3*). The chemical shifts of the zinc-binding residues as well as the cross-peak patterns of the NOEs of the zinc-binding residues were also very similar to those of the individually solved domains. In B-box 1, one zinc atom was coordinated by residues Cys119, Cys122, Cys142, and Cys145, while the other was coordinated by Cys134, Cys137, His150, and His159. In B-box2, one zinc atom was coordinated by residues Cys175, His178, Cys195, and Cys198, and the other was coordinated by residues Cys187, Asp190, His204, and His207.

The tertiary structures of the MID1 tandem B1B2 domains were calculated with CYANA 2.1 (*20*) based on 1026 NOEs, 22 hydrogen bonds, 48 phi (ϕ) and psi (ψ), and 41 Zn-protein restraints. Twenty structures with the lowest target function values (<1.0), NOE violations <0.1 Å, dihedral angles <2°, and van der Waals violations <0.2 Å were selected. Input data and statistics of the calculated structures are summarized in Table 1. The root-mean-square deviation (rmsd) for the superposition of the backbone atoms (N, Cα, and C) for residues Val117 to Ala209, excluding residues Pro151 to Gly158 and Glu163 to Leu173, was 0.45 ± 0.10 Å (Table 1 and Figure 2a). The rmsd of the superposition for all heavy atoms for these same set of residues was 0.8 ± 0.10 Å. Evaluation of the structures with PROCHECK (*22*) revealed that 82% of the structured residues were in the most favored regions of the Ramachandran plot with the remaining 18% in favored regions (Table 1). These percentages are above the average of other RING structures determined by both NMR spectroscopy and X-ray crystallography. For example, a comparison of structured residues in the most favored regions of the Ramachandran plot for all RING domains determined by NMR spectroscopy revealed an average value of 71 ± 9%. Specifically, the BARD1-BRCA1 and HDM2 dimers show 68 and 72%, respectively, of their structured residues in the most favored regions (*12*, *13*). It is worth

Table 1: Statistics of MID1 B1B2 Structure Calculations

NOE Distance Restraints	
intra-residue ($\|i-j\|=0$)	412
sequential ($\|i-j\|=1$)	261
medium-range ($\|i-j\|=2-4$)	162
long-range ($\|i-j\|>4$)	191
total NOEs	1026
dihedral angle restraints ($\phi\psi$)[a]	96
hydrogen-bond restraints	22
zinc-protein restraints	41
total restraints	1185
Violations	
distance restraint >0.2 Å	0
VDW 0.15−0.3 Å	9[b]
dihedral >5°	0

Ramachandram plot (%)	all residues	structured residues[c]
most favored	74.2 ± 2.2	82.3 ± 1.0
additionally allowed	23.5 ± 3.0	17.7 ± 2.0
generously allowed	2.0 ± 1.0	0.0
disallowed	1.0 ± 1.0	0.0

Overall precision of an ensemble of 20 structures[d]

	B1B2	B1	B2
backbone atoms[e]	0.45 ± 0.1	0.33 ± 0.1	0.25 ± 0.1
heavy atoms[f]	0.80 ± 0.1	0.69 ± 0.1	0.60 ± 0.1

[a] Dihedral angles estimated using TALOS based on NH, ^{15}N, Hα, Cα, and Cβ chemical shifts of each amino acid. [b] All VDW violations arise from S−Zn restraints, due to the larger radius of zinc in CYANA 2.1. [c] The structured residues include Val117 to His150, His159 to Leu1161, and Met174 to Ala110. These values were calculated with Procheck. [d] Residues Ser90 to Lys116, Pro151 to Gly158, and Glu163 to Leu173 were omitted from the superposition because of limited long-range NOEs between these residues and the rest of the protein. Root-mean-square deviation (rmsd) values were calculated with CYANA 2.1. [e] Backbone atoms include backbone N, Cα, and CO. [f] Heavy atoms include both backbone and side-chain non-hydrogen heavy atoms.

noting that the MID1 tandem B1B2 domains are small zinc-binding domains with a relatively low proportion of residues in well-defined secondary structural elements. Only 30% of residues is in β-strands and α-helices. A further 30% of residues is unstructured, with the remaining residues in structured loops and turns.

Both B-boxes adopt RING-like ββα motifs, each with two bound zinc atoms (Figure 2d). The determination of two bound zinc atoms by the B-box domains was previously described (*2*, *3*). The unstructured N-terminal residues lead into a large hairpin turn that sits above the α-helix, presenting two zinc-binding residues to the first helical turn, which itself contains two zinc-binding residues. The structured loops within the regions Val131 to Tyr141 and Met183 to Ile194 each contain two short antiparallel β-strands that are positioned almost perpendicular to the helix. The turns separating these β-strands both contain two zinc-binding residues, with the B-box1 turn having Cys134 and Cys137 and B-box2 having Cys187 and Asp190. The large relatively unstructured loop following the helix of B-box1 contains two zinc-binding histidines. This loop proceeds away from the core of B-box1 and leads into the other large turn containing zinc-binding residues Cys175 and His178 that coordinates a zinc ion with the two cysteines from the first helical turn of the B-box2 helix (Figure 2d). Comparison of the independently solved B-box1 and B-box2 structures with the respective domains in the tandem globular structure revealed that they were both essentially identical. The rmsd values of the superposition of the backbone atoms of just the B-box1 and B-box2 domains with their respective domain within B1B2 were 0.33 ± 0.1 and 0.25 ± 0.1 Å, respectively (Figure 2b,c).

The interface between the B-box domains was identified by 26 NOEs between the side-chain protons of residues Ala130 and Asp191, Lys132 and Gln192, Thr133 and Asp190, Ser140 and Asp190, and Ile162 and Ile194 (Figures 2e and 3). The interfacing residues on B-box2 are located on the turn separating the β-strands, while those of B-box1 are on the outer surface of the two-stranded β-sheet (Figure 2e). As a result, the two sets of β-sheets are perpendicular to each other and not positioned in a fashion that resulted in any symmetry, which was observed for the hetero- and homo-RING dimers (Figure 4) (*12*−*14*). Careful analysis of the data did not reveal any NOEs that would allow B-box domains to interact in a similar fashion as the RING dimers (Figure 3). Thus, while our B-box domains interact in a fashion reminiscent of RING dimers, the orientation is slightly different. The interaction is also consistent with mutagenesis studies (see Discussion). The area of the interface between the B-box domains was calculated using the program CCP4 to be ∼188 Å^2 (∼377 Å^2 total buried surface area or 17% of the total surface).

To determine the effect of the interaction of the tandem B-boxes on the thermal stability of the B-box domains, the melting temperature (T_m) was monitored using a differential scanning calorimeter (Model N-DSCII, Calorimetry Science Corp). The T_m values for B-box1 and B-box2 were determined to be ∼52 and 47 °C, respectively, while the T_m value for the tandem B-box domains was 59 °C. To verify that the higher T_m value for B1B2 was not simply due to its larger size as compared to the individual domains, we used ^{1}H−^{15}N HSQC experiments to follow the ^{1}H−^{15}N peaks of B-box1, B-box2, and B1B2 to monitor folding with an increasing temperature. The unfolding of the tertiary structures of the B-box domains was identified by monitoring peak disappearance due to solvent exchange and line-shape broadening and the degeneracy of ^{1}H−^{15}N proton chemical shifts. At 55 °C, most of the peaks for the individual B-box1 and B-box2 domains were gone, while most were present in the tandem B1B2 domains. This observation suggests that the enhanced thermal stability of the individual domains in tandem is most likely due to the interaction of the B-box domains.

DISCUSSION

Globular Structure of B1B2 Is Similar to That of RING Heterodimers. The B-box interface was determined by 26 NOEs between 10 amino acids located on the structured loops of each domain. The tandem globular structure is reminiscent of the intermolecular association seen for the two heterodimeric RING structures: the RING heterodimer of BARD1 and BRCA1 (*12*) and the polycomb group protein, Bmi-1, and Ring1B polycomb group ubiquitin ligase (*14*). In addition, the HDM2 homodimeric RING domains also adopted a similar structure (*13*). In all the RING dimers, the domains interact via residues located on the turn separating the two short β-strands on the structured loops (Figure 4). The orientation and interface of both hetero- and homo-RING dimers are remarkably similar. In addition, in

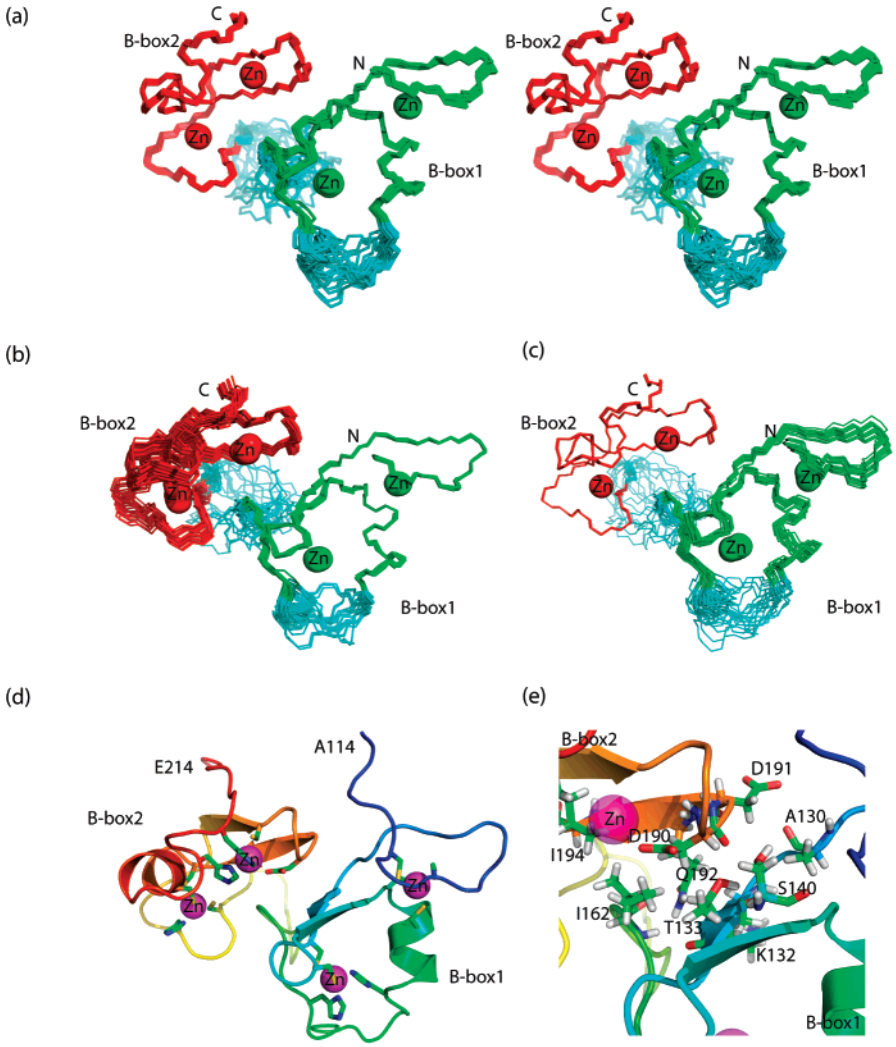

FIGURE 2: Solution structure of MID1 B1B2. (a) Stereoview of 20 structures showing the superposition of backbone Cα, C, and N atoms of the structured amino acid of both domains. The zinc atoms are shown as spheres and labeled. Residues Ser90-Lys116 are unstructured and not shown. B-Box1 is green, B-box2 is red, and the unstructured residues (Pro151 to Pro157 and Ile162 to Leu173) are cyan. (b) Superposition of the backbone atoms of the structured residues (Val117 to His150 and His159 to Leu161) of just the B-box1 domain. (c) Superposition of the backbone atoms of the structured residues (Met174 to Ala210) of just the B-box2 domain. The small increase in the precision of the positions of the non-superimposed domain indicates a small degree of flexibility between the B-box domains. Residues Val117-Glu214 are shown for a−c. (d) Ribbon representation of B1B2 (Ala114 to Glu214) with the zinc ions shown as magenta spheres. Atom types of zinc-coordinating residues are color coded: yellow is sulfur, green is carbon, blue is nitrogen, and red is oxygen. (e) Close-up view of the 10 residues that show 26 inter-domain NOEs. These residues are located at the interface of the B-box domains.

both hetero-RING structures, the proteins interact via a four-helix bundle, with each RING protein providing two helices. Omitting the residues forming the helical bundle, the total buried surface area and area of the interface of BRCA1-BARD1 was determined to be ~168 and ~84 Å^2 (8% total surface), respectively. A similar value was obtained for Bmi-1-Ring1B, although the Ring1B RING domain has a 16 amino acid N-terminus that wraps around the Bmi-1 RING domain (*14*). In contrast, the interface between the B-boxes is approximately twice as large as the hetero-RING dimers, with the two B-box domains packing slightly differently to the RING domains. Instead of residues on the turn interacting, residues on the turn separating the β-strands of B-box2 pack against the outer surface of the two-stranded antiparallel β-sheet of B-box1. This interaction orients the two B-boxes ~90° rotated along the *y*-axis, based on the orientation of the helices, as compared to the RING heterodimers (Figures 2e and 4a). The two sets of β-sheets are positioned perpendicular to each other and therefore do not have a pseudo-*C*2 axis of symmetry observed for the hetero- and homo-RING dimers (Figure 4). Therefore, the location of the interaction of B-box1 with B-box2 is very similar to that of BARD1 or Bmi-1 interacting with their respective RING domains, but the orientation of B-box2 is different. After superimposition of B-box1 with the BRCA1, Ring1B, and HDM2 RING domains, and comparison of the position of B-box2 with the BARD1, Bmi1, and HDM2 RINGs, we note in the RING domains the presence of an additional C-terminal β-strand in the position equivalent to where the short two-stranded β-sheet of B-box2 is located (Figure 4). There is no propensity for a third C-terminal β-strand in the MID1 B-box1. On the basis of our B1B2 structure, we do not believe that B-box2 could pack against B-box1 in its current orientation with the presence of an additional C-terminal β-strand in B-box1. In addition, it is also possible that the four-helix bundle in the RING heterodimers could influence their position and orientation. Consistent with this notion, the orientation of the RING domains in the HDM2 ho-

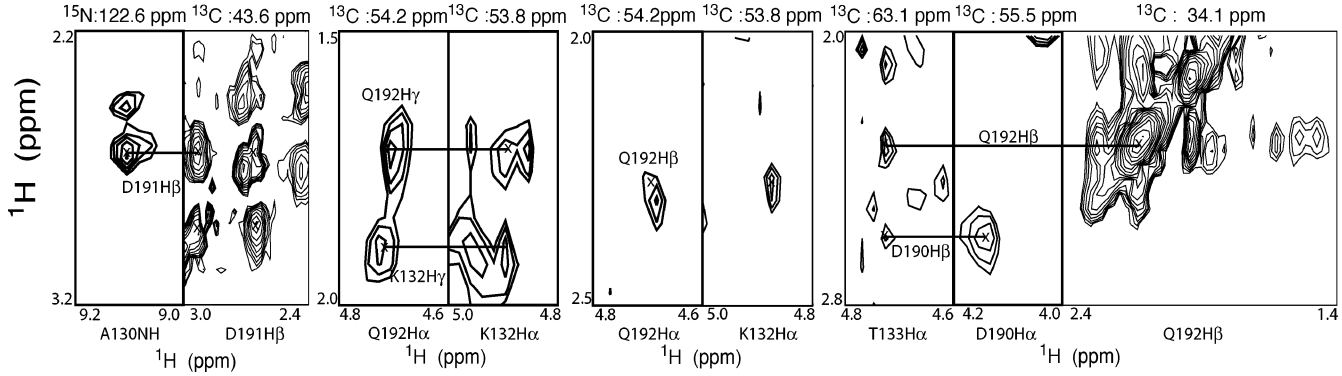

FIGURE 3: ^{15}N- and ^{13}C-slices from ^{1}H−^{15}N HSQC-NOESY and ^{1}H−^{13}C HSQC-NOESY spectra showing NOEs that define the interface and orientation of the interaction of the B-box domains. Residues Ala130, Lys132, and Thr133, which are located on the outer surface of the B-box1 β-sheet, show NOEs with residues Asp191 and Asp190, which are located on the turn separating the β-strands on B-box2.

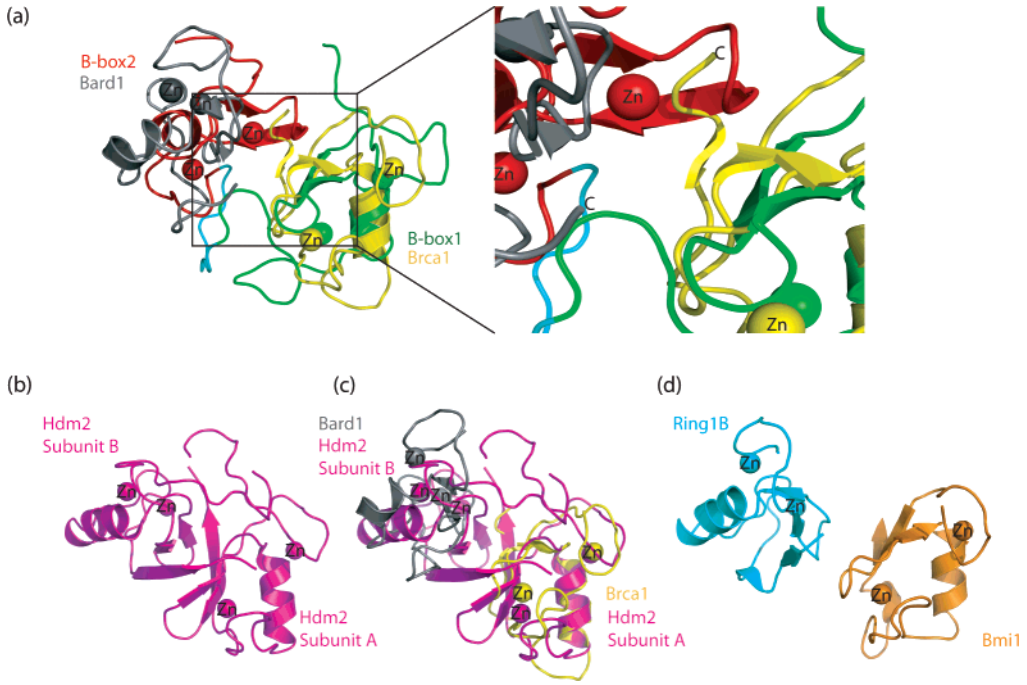

FIGURE 4: Comparison of MID1 B1B2 with RING hetero- and homo-dimers. (a) Ribbon representation of the MID1 tandem B1B2 structure shown with the B-box1 domain (green; Ala130 to Leu146 representing the structured loop and α-helix) aligned structurally with the BRCA1 RING domain (yellow; residues Pro34 to Lys50). The relative orientation of B-box2 (red) and BARD1 (gray) are shown. B-Box2 is closer to B-box1 than the BARD1 RING is to BRCA1, and it is rotated by ~90° when compared to the BARD1 RING helix. This difference in orientation is hypothesized to be partly due to the presence of the third β-strand in the BRCA1 RING domain (see magnified image), which would sterically block the BARD1 RING domain from packing in a similar orientation as B-box2. The zinc atoms are shown as spheres, colored to correspond to the domain with which they are coordinated. (b) Ribbon representation of the HDM2 homodimer (*13*). (c) Tertiary structural alignment of the BRCA1-BARD1 hetero-RING dimer with the HDM2 homodimer reveals that the orientation of BARD1 and one monomer of HDM2 is different by ~45° with respect to the helix. (d) Ribbon representation of the RingB1-Bmi1 X-ray structure (*14*). This structure superimposed very well with the BRCA1-BARD1 RING dimers.

modimer, which does not have a four-helix bundle, is slightly different from that seen in the heterodimers, and the total interface area between the RING domains is larger (368 Å), more like the interaction of the tandem B-boxes in MID1. On the other hand, it is also wholly possible that because the B-box domains have not been shown to possess E3 ligase activity so far, the mode of interaction of B-box2 with B-box1 may be essential for, or limited and unique to, regulating the function of B-box1. In the case of MID1, this may impact its ability to bind Alpha4 and recruit PP2Ac to the microtubule network.

Biological Significance of MID1 Tandem B-Box Domains. This report represents the first description of a tandem B-box structure that characterizes many RBCC/TRIM and non-RBCC proteins. The MID1 B1B2 structure shows a quaternary structure reminiscent of the intermolecular RING heterodimers, suggesting possible evolutionary constraints on the function or role of RING-type folds whether the domains are present in two independent interacting protein partners or within the same protein. Supported by T_m studies, the more thermally stable B1B2 might mirror the situation in hetero-RING dimers, where a more stable RING E3 ligase can interact more efficiently with the E2 ligase, thus enhancing E3 activity (*23*, *24*).

On the other hand, as noted, one of the roles of B-box2 may be to modulate the function of B-box1, and its mode of

action may be similar to the way RING domains affect the function of each other in the heterodimeric state. This notion is strengthened by the observation that, irrespective of the species, the order of B-boxes in the tandem configuration (i.e., a type 1 B-box followed by a type 2 B-box) does not vary among the proteins that possess them (*1*). Furthermore, the interface between the B-box domains is relatively small and lined with charged residues, and thus, the interaction could also potentially be modulated. To this end, the RING-like folds of the B-boxes and the nature of their interaction raise the possibility that B-box2 could also interface with RING domains. In fact, many RBCC/TRIM proteins possess only a single B-box domain, and these are invariably type 2 B-box domains. In these proteins, this domain is always positioned immediately C-terminal to a RING domain and thus in a similar configuration to the tandem B-boxes(*1*). Ongoing studies are being carried out to investigate as to whether this might be a common mechanism by which to regulate E3 activity in proteins with RING-type folds.

While the functions of most B-box domains remain unclear, indirect roles for a few type 2 B-boxes have been reported, including a putative regulatory role in the antiviral activity of TRIM5 (*25*, *26*) and, in MID1, influencing the strength of interaction between the adjacent B-box1 and the protein phosphatase 2A regulator, Alpha4 (*6*). In the latter example, it is possible that the interaction surface between B-box1 and B-box2 partially overlaps that required for tight binding of Alpha4. In this regard, six mutations within the MID1 B-boxes have been found in patients with Opitz syndrome: ΔCys137, Cys195Phe, Cys142Ser, Cys145Tyr, Ala130Thr, and Ala130Val (*9*−*11*). While the first four mutations involve residues that are critical for coordinating the zinc ions and therefore would be expected to perturb the folding and formation of the cross-brace motifs of the respective B-box domain in which they reside (*2*), the other two mutations apparently arose de novo in the patients and both involve substitutions of Ala130, which is positioned in the interface between the B-box domains (Figure 2e). Apart from the zinc-coordinating residues, Ala130 is the most highly conserved residue among all B-box1 domains being present in almost all such domains, with notable exceptions including serine (e.g., in the MID1-like TRIM36) and valine (e.g., in TRIM45) (*2*). Recent studies have provided some evidence that at least the Ala130Thr mutant of MID1 can still bind microtubules but has a significantly reduced affinity for Alpha4 (*27*). In contrast, the consequences of the Ala130Val mutation are not yet known, although it is likely that the overall structure of the B-box1 also remains intact since valine is found in the equivalent position in the TRIM45 B-box1. Curiously, a fortuitously generated B-box2 mutation (Gln192Arg) was recently suggested to disrupt Alpha4 binding to B-box1 based on co-immunofluorescence data (*27*). On our structure, this residue is also positioned at the interface between the B-boxes, supporting the notion that the B-box1−B-box2 interaction is important for overall MID1 function. The reported effects of these mutations provide additional support for our B1B2 tertiary structure, where residues on the turn separating the two β-strands of B-box2 (Gln192) are packed against residues on the outer surface of the β-strands of B-box1 where Ala130 is located (Figure 2e). However, further studies on the structure and function of tandem B-box domains need to be pursued to understand as to whether such mutations perturb key residues required for the direct binding of Alpha4 or impact on higher-order quaternary structures (i.e., regulated binding of Alpha4 to B-box1).

ACKNOWLEDGMENT

We thank Dr. Chang-an Yu (Oklahoma State University) for help and the use of his DSC spectrometer and Kevin McAbee for computer help.

REFERENCES

1. Short, K. M., and Cox, T. C. (2006) Sub-classification of the RBCC/TRIM superfamily reveals a novel motif necessary for microtubule binding, *J. Biol. Chem. 281*, 8970−8980.
2. Massiah, M. A., Simmons, B. N., Short, K. M., and Cox, T. C. (2006) Solution structure of the RBCC/TRIM B-box1 domain of human MID1: B-box with a RING, *J. Mol. Biol. 358*, 532−545.
3. Massiah, M. A., Matts, J. A. B., Short, K. M., Simmons, B. N., Singireddy, S., Yi, Z., and Cox, T. C. (2007) Solution structure of the MID1 B box2 CHC(D/C)C2H2 domain: Insight into an evolutionary conserved RING fold, *J. Mol. Biol. 369*, 1−10.
4. Short, K. M., Hopwood, B., Yi, Z., and Cox, T. C. (2002) Mid1 and Mid2 homo- and heterodimerize to tether the rapamycin-sensitive PP2A regulatory subunit, Alpha 4, to microtubules: Implications for the clinical variability of X-linked Opitz GBBB syndrome and other developmental disorders, *BMC Cell Biol. 3*, 1.
5. Schweiger, S., and Schneider, R. (2003) The MID1/PP2A complex: A key to the pathogenesis of Opitz BBB/G syndrome, *Bioessays 25*, 356−366.
6. Trockenbacher, A., Suckow, V., Foerster, J., Winter, J., Krauss, S., Ropers, H. H., Schneider, R., and Schweiger, S. (2001) MID1, mutated in Opitz syndrome, encodes an ubiquitin ligase that targets phosphatase 2A for degradation, *Nat. Genet. 29*, 287−294.
7. Liu, J., Prickett, T. D., Elliott, E., Meroni, G., and Brautigan, D. L. (2001) Phosphorylation and microtubule association of the Opitz syndrome protein mid-1 is regulated by protein phosphatase 2A via binding to the regulatory subunit alpha 4, *Proc. Natl. Acad. Sci. U.S.A. 98*, 6650−6655.
8. Cox, T. C., Allen, L. R., Cox, L. L., Hopwood, B., Goodwin, B., Haan, E., and Suthers, G. K. (2000) New mutations in MID1 provide support for loss of function as the cause of X-linked Opitz syndrome, *Hum. Mol. Genet. 9*, 2553−2562.
9. Ferrentino, R., Bassi, M. T., Chitayat, D., Tabolacci, E., and Meroni, G. (2007) MID1 mutation screening in a large cohort of Opitz G/BBB syndrome patients: Twenty-nine novel mutations identified, *Hum. Mutat. 28*, 206−207.
10. Pinson, L., Auge, J., Audollent, S., Mattei, G., Etchevers, H., Gigarel, N., Razavi, F., Lacombe, D., Odent, S., Le Merrer, M., Amiel, J., Munnich, A., Meroni, G., Lyonnet, S., Vekemans, M., and Attie-Bitach, T. (2004) Embryonic expression of the human MID1 gene and its mutations in Opitz syndrome, *J. Med. Genet. 41*, 381−386.
11. So, J., Suckow, V., Kijas, Z., Kalscheuer, V., Moser, B., Winter, J., Baars, M., Firth, H., Lunt, P., Hamel, B., Meinecke, P., Moraine, C., Odent, S., Schinzel, A., van der Smagt, J. J., Devriendt, K., Albrecht, B., Gillessen-Kaesbach, G., van der Burgt, I., Petrij, F., Faivre, L., McGaughran, J., McKenzie, F., Opitz, J. M., Cox, T., and Schweiger, S. (2005) Mild phenotypes in a series of patients with Opitz GBBB syndrome with MID1 mutations, *Am. J. Med. Genet. A 132*, 1−7.
12. Brzovic, P. S., Rajagopal, P., Hoyt, D. W., King, M. C., and Klevit, R. E. (2001) Structure of a BRCA1-BARD1 heterodimeric RING-RING complex, *Nat. Struct. Biol. 8*, 833−837.
13. Kostic, M., Matt, T., Martinez-Yamout, M. A., Dyson, H. J., and Wright, P. E. (2006) Solution structure of the HDM2 C2H2C4 RING, a domain critical for ubiquitination of p53, *J. Mol. Biol. 363*, 433−450.
14. Li, Z., Cao, R., Wang, M., Myers, M. P., Zhang, Y., and Xu, R. M. (2006) Structure of a Bmi-1-Ring1B polycomb group ubiquitin ligase complex, *J. Biol. Chem. 281*, 20643−20649.

15. Delaglio, F., Grzesiek, S., Vuister, G. W., Zhu, G., Pfeifer, J., and Bax, A. (1995) NMRPipe: A multidimensional spectral processing system based on UNIX pipes, *J. Biomol. NMR 6*, 277−293.
16. Goddard, T. D., and Kneller, D. G. *SPARKY 3*, University of California, San Francisco.
17. Cornilescu, G., Delaglio, F., and Bax, A. (1999) Protein backbone angle restraints from searching a database for chemical shift and sequence homology, *J. Biomol. NMR 13*, 289−302.
18. Summers, M. F., Henderson, L. E., Chance, M. R., Bess, J. W., Jr., South, T. L., Blake, P. R., Sagi, I., Perez-Alvarado, G., Sowder, R. C., III, Hare, D. R. et al. (1992) Nucleocapsid zinc fingers detected in retroviruses: EXAFS studies of intact viruses and the solution-state structure of the nucleocapsid protein from HIV-1, *Protein Sci. 1*, 563−574.
19. Wang, B., Alam, S. L., Meyer, H. H., Payne, M., Stemmler, T. L., Davis, D. R., and Sundquist, W. I. (2003) Structure and ubiquitin interactions of the conserved zinc finger domain of Npl4, *J. Biol. Chem. 278*, 20225−20234.
20. Guntert, P. (2004) Automated NMR structure calculation with CYANA, *Methods Mol. Biol. 278*, 353−378.
21. Auld, D. S. (2001) Zinc coordination sphere in biochemical zinc sites, *BioMetals 14*, 271−313.
22. Laskowski, R. A., MacArthur, M. W., Moss, D. S., and Thornton, J. M. (1993) PROCHECK: A program to check the stereochemical quality of protein structures, *J. Appl. Crystallogr. 26*, 283−291.
23. Mallery, D. L., Vandenberg, C. J., and Hiom, K. (2002) Activation of the E3 ligase function of the BRCA1/BARD1 complex by polyubiquitin chains, *EMBO J. 21*, 6755−6762.
24. Xia, Y., Pao, G. M., Chen, H. W., Verma, I. M., and Hunter, T. (2003) Enhancement of BRCA1 E3 ubiquitin ligase activity through direct interaction with the BARD1 protein, *J. Biol. Chem. 278*, 5255−5263.
25. Javanbakht, H., Diaz-Griffero, F., Stremlau, M., Si, Z., and Sodroski, J. (2005) The contribution of RING and B-box 2 domains to retroviral restriction mediated by monkey TRIM5alpha, *J. Biol. Chem. 280*, 26933−26940.
26. Perez-Caballero, D., Hatziioannou, T., Yang, A., Cowan, S., and Bieniasz, P. D. (2005) Human tripartite motif 5alpha domains responsible for retrovirus restriction activity and specificity, *J. Virol. 79*, 8969−8978.
27. Orgillés, B. A. (2006) Characterisation of MID1/W4 multiprotein complex. Thesis for doctor rerun naturalium, Freie Universität Berlin, Berlin, http://www.diss.fuberlin.de/2006/660/.

BI7018496